Journal of Quantitative Spectroscopy & Radiative Transfer 187 (2017) 453–460

Contents lists available at ScienceDirect

Journal of Quantitative Spectroscopy & Radiative Transfer

journal homepage: www.elsevier.com/locate/jqsrt

Pressure-dependent water absorption cross sections for exoplanets and other atmospheres

Emma J. Barton [a], C. Hill [a], Sergei N. Yurchenko [a], Jonathan Tennyson [a,*], Anna S. Dudaryonok [b], Nina N. Lavrentieva [b]

[a] Department of Physics and Astronomy, University College London, London WC1E 6BT, UK
[b] V. E. Zuev Institute of Atmospheric Optics SB RAS, 1, Sq. Academician Zuev, 634021 Tomsk, Russia

ARTICLE INFO

Article history:
Received 3 September 2016
Received in revised form
21 October 2016
Accepted 27 October 2016
Available online 3 November 2016

Keywords:
Water
Cross sections
Pressure broadening
Atmospheres
Extrasolar planets
BT2
Composition

ABSTRACT

Many atmospheres (cool stars, brown dwarfs, giant planets, extrasolar planets) are predominately composed of molecular hydrogen and helium. $H_2{}^{16}O$ is one of the best measured molecules in extrasolar planetary atmospheres to date and a major compound in the atmospheres of brown-dwarfs and oxygen-rich cool stars, yet the scope of experimental and theoretical studies on the pressure broadening of water vapour lines by collision with hydrogen and helium remains limited. Theoretical H_2- and He-broadening parameters of water vapour lines (rotational quantum number J up to 50) are obtained for temperatures in the range 300–2000 K. Two approaches for calculation of line widths were used: (i) the averaged energy difference method and (ii) the empirical expression for $J'J''$-dependence. Voigt profiles based on these widths and the BT2 line list are used to generate high resolution ($\Delta\tilde{\nu} = 0.01$ cm^{-1}) pressure broadened cross sections for a fixed range of temperatures and pressures between 300 and 2000 K and 0.001–10 bar. An interpolation procedure which can be used to determine cross sections at intermediate temperature and pressure is described. Pressure broadening parameters and cross sections are presented in new ExoMol format.

1. Introduction

The ExoMol project aims to provide comprehensive line lists of molecular transitions appropriate for molecules in hot atmospheres such as those found in exoplanets, brown dwarfs and cool stars [1]. Until recently the ExoMol database did not include any information on the pressure broadening of molecular lines despite the known importance of pressure effects in these environments [2]. The scope of the ExoMol database is being extended to systematically provide this additional data and other supplementary data in order to maximise the usefulness of the line lists [3]. A major new feature is the inclusion, albeit at a fairly crude level for most molecules, of pressure-broadening parameters and pressure-dependent absorption cross sections.

$H_2{}^{16}O$ is one of the few molecules detected in the atmosphere of an exoplanet to date [4,5]. In particular it has been identified in the atmospheres of several hot extrasolar giant planets including HD189733b [6–11], GJ 436b [12,13], HD 209458b [14,15], XO-1b [16,15], HAT-P-1b [17], HD 179949b [18], WASP-19b [19], WASP-12b [20] and planets orbitting HR 8799 [21,22]. Test model calculations have shown that including pressure broadening of the water spectrum significantly alters the observed spectrum of transiting hot Jupiter exoplanet [2].

Prior to the discovery of exoplanets, $H_2{}^{16}O$ was already known to be a component of the atmospheres of cool stars and brown dwarfs [23–26], where it can dominate the observed spectrum [27]. Recent discoveries have focused very cold brown dwarfs: Faherty et al. [28] made a tentative detection of water clouds in WISE J085510.83-071442.5 and Skemer et al. [29] detected water and clouds in the cold brown dwarf *WISE* 0855.

$H_2{}^{16}O$ is one of the few molecules contained in the current release of HITEMP [30] which contains a comprehensive set of air- and self-broadening parameters. These were obtained using a diet based on physical principles and statistics [31] which had a strong bias toward near-room temperatures. As the bulk of the atmosphere of giant exoplanets and cool stars is composed of a H_2 rich H_2-He mix, molecular opacities in atmospheric models for these objects should incorporate pressure broadening due to H_2 and He.

A number of works, reviewed in the next section, have provided pressure broadening parameters for broadening of $H_2{}^{16}O$ by H_2 and/or He for this purpose, although the spectral, temperature and pressure coverage is far from comprehensive. Altogether, detailed information for broadening of water vapour lines by H_2 and He is available for around 1100 and 5000 lines respectively, while

* Corresponding author.
E-mail address: j.tennyson@ucl.ac.uk (J. Tennyson).

http://dx.doi.org/10.1016/j.jqsrt.2016.10.024
0022-4073/

the most complete line list for water to date (BT2, [32]) contains around half a billion lines which is sufficiently complete for temperatures up to 3000 K. The temperature coverage, although appreciable for broadening by H_2 (40–1500 K), is more limited for broadened by He (83–600 K). Conversely the pressure coverage for broadening by He (up to 3 atm) is more extensive than for broadening by H_2 (up to 1330 mbar ≈ 1.3 atm).

The first aim of this work is to provide $H_2{}^{16}O$–H_2 and $H_2{}^{16}O$–He pressure broadening parameters suitable for temperatures up to 2000 K and pressures up to 10 bar. These parameters can be used to generate a pressure and temperature dependent Lorentzian half-width for every line in the BT2 line list, or indeed any water line list with at least rotational angular momentum ($J' - J''$) quantum assignments.

The implementation of full line lists in atmospheric modelling codes, although ideal, is often not practical due to their sheer size [33]. Hence the second aim of this work is to provide pressure-dependant absorption cross sections based on Voigt profiles for $H_2{}^{16}O$ in a mixed H_2/He (85/15%) environment for a range of temperatures (T=300–2000 K) and pressures (P=0.001–10 bar) relevant to exoplanet and cool star atmospheres.

2. Previous work

For the $H_2{}^{16}O$-H_2 system the most extensive experimental study was performed by Brown and Plymate [34] who derived pressure broadened widths for 630 lines in the range 55–4045 cm^{-1} at room temperature. Other exclusively room temperature measurements have been carried out by Steyert et al. [35] (39 lines in the range 380–600 cm^{-1}), Brown et al. [36] (4 lines around 1540 cm^{-1}), Golubiatnikov [37] (1 line at 183 GHz), Lucchesinia et al. [38] (15 lines in the range 820–830 nm), and Zeninari et al. [39] (6 lines around 1.39 μm). The temperature and/or pressure dependence of the collision induced widths for selected (2–12) $H_2{}^{16}O$ lines has been investigated by a handful studies [39–42]. The works considering the widest range of temperatures and pressures are those by Langlois et al. [41] and Zeninari et al. [39] respectively. Langlois et al. combined two experimental set-ups, one incorporating a temperature controlled static cell (limited to 450 K), the other a pressure driven shock tube, to determine the temperature dependence of the pressure broadened widths of twelve $H_2{}^{16}O$ lines over the range 300–1200 K with an expected accuracy of ±25%. The dependence could be roughly represented by a power law of decreasing collision induced line width with increasing temperature. Zeninari et al. made measurements of six $H_2{}^{16}O$ lines at several pressures between 6 and 1330 mbar (ambient pressure ≈ 1000 mbar) and concluded that the dependence could be described as a linear increase in collision induced line width with pressure.

Theoretically determined pressure broadened widths and their temperature dependence are available from Gamache et al. [43], Faure et al. [44] and Drouin and Wisenfeld [45]. Drouin and Wisenfeld focused on three lines at cold temperatures (below 200 K) while Gamache, Lynch et al. aimed to provide information for hundreds of lines suitable for high temperature applications. The maximum temperature considered by Faure et al. was hotter (1500 K vs 750 K) though Gamache et al. produced parameters for more lines (386 vs 228). All three works focused on rotational transitions.

Several of the studies already mentioned [38,35–37,43,40,42,39] also reported parameters for the $H_2{}^{16}O$-He system. Although the most extensive studies of He-broadening coefficients of $H_2{}^{16}O$ have been performed by Petrova and co-workers [46–48], and Solodov and Starikov [49,50]. Each of these works presented measurements of pressure broadened widths for tens of lines belonging to strong vibrational bands including $\nu_2 + \nu_3$ [49,50,47,48], $\nu_1 + \nu_2$ [50,47,48], $\nu_1 + \nu_2 + \nu_3$ [46,47] and $2\nu_3$ and $\nu_1 + 2\nu_1$ [48] at room temperature and varying pressures. All found the pressure dependence to be linear (up to 3 atm [47,48]). Petrova et al. [47] combined their own measurements with literature data to determine the vibrationally and rotationally dependent intermolecular potential for the $H_2{}^{16}O$-He system. This potential was used by Petrova et al. [47,48] to compute, and fit an analytical expression to, helium pressure broadened width for transitions belonging to 11 and 13 vibrational bands respectively with rotational quantum numbers J and K_a up to 14 in the temperature interval $83 \le T \le 600$ K. The temperature dependence in the model was refined by comparison to previous temperature dependent studies by Goyette and De Lucia [51] (1 line at 183 GHz, 80–600 K) and Godon and Bauer [52] (2 lines at 183 and 380 GHz, 300–390 K). In addition room temperature pressure broadened widths for $H_2{}^{16}O$-He have been measured by Lazarev et al. [53] (1 line at 14,397.4 cm^{-1}), Poddar et al. [54] (14 lines in the range 11,988–12,218 cm^{-1}), Claveau et al. [55] (14 lines in the range 1850–2140 cm^{-1}) and Claveau and Valentin [56] (10 lines in the range 1170–1440 cm^{-1}). Claveau et al. and Claveau and Valentin also investigated narrowing due to dynamic confinement (Dicke narrowing [57,58]).

3. Calculation of H_2 and He pressure induced line widths of $H_2{}^{16}O$ spectral lines

3.1. Theoretical techniques used

Two calculation techniques are used to determine the $H_2{}^{16}O$-H_2 and $H_2{}^{16}O$-He Lorentzian half-widths. These techniques distinguish between rigorous quantum numbers, namely the total angular momentum J and total symmetry (Γ_{tot}), which corresponds to parity and ortho/para designation, and approximate projections of the rotational motion (K_a,K_c). The techniques are:

1. The averaged energy difference (AED) method [59] is used in cases where the complete set of quantum numbers (both rigorous and approximate) of a transition are known.
2. The $J'J''$- dependence technique [60] has been applied in cases where only rigorous (total angular momentum J and total symmetry) were known.

These approaches are described in detail in the respective papers, thus only the main features are outlined below.

The averaged energy difference method allows the calculation of line widths of asymmetric top molecules with approximately the same precision as in modern theoretical and experimental methods without the need for a complicated calculation scheme. The approach is based on matching the so called coupled energy state difference with a line broadening value. Based on the modified Robert-Bonamy formalism, the expression for the half-widths γ_{if} is given by [61,62]:

$$\gamma_{if} = \frac{n_b}{2\pi c}\int_0^{+\infty} v\, f(v)\, dv \int_0^{+\infty} 2\,\pi\, b\, db\left[1 - \cos(S_1 + \mathrm{Im}(S_2))e^{-\mathrm{Re}(S_2)}\right] \quad (1)$$

where indices i and f specify initial and final energy states, n_b is the number density of perturbers, b is the impact parameter, v is the relative initial velocity and $f(v)$ is the Maxwell Boltzmann distribution function [59,61,62]. Real S_1 and complex $S_2 = \mathrm{Re}(S_2) + i\,\mathrm{Im}(S_2)$ are the first and second order terms in the expression for the scattering matrix. These terms depend on collision dynamics, the intermolecular potential and on the ro-vibrational states of the molecule (and collision induced transitions between these states). Expressions for S_1 and S_2 can in found in Refs. [59,63–65].

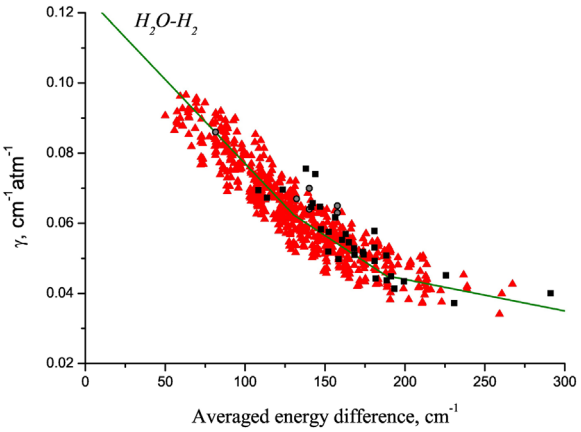

Fig. 1. Dependence of $H_2{}^{16}O$-H_2 broadening coefficients on averaged coupled energy state difference at 296 K; experimental data: rotational band and fundamentals [34], red triangles; rotational band [35], black squares; $\nu_1 + \nu_3$ and $2\nu_2$ [41], gray circles. (For interpretation of the references to color in this figure legend, the reader is referred to the web version of this article.)

The aim is to estimate how values of $Re(S_2)$ vary with different lines of interest. Coupled energy state differences $\tilde{\omega}_{if}$ between an $H_2{}^{16}O$ line of interest and other coupled lines ($\tilde{\omega}_{if}$ is defined explicitly in [59]) are derived for thousands of lines. The averaged energy differences for lines with experimentally-determined collision-induced widths are then used to match averaged state energy differences to line broadening values using a fitting formula.

The dependence of broadening parameters on the averaged energy difference of the coupled states is smooth. Fig. 1 illustrates this for the $H_2{}^{16}O$-H_2 line widths. This figure demonstrates that one can estimate corresponding widths with a simple fitting formula. For other systems such N_2 broadening of water the observed data has been found to lie almost exactly on a smooth curve [66]; here the scatter reflects, at least in part, uncertainty in the experimental data. The reconstructed widths obtained from the fitting formula agree well with the experimental values as shown in Fig. 2 for $H_2{}^{16}O$-H_2. This method requires assignment to normal modes (via quantum numbers ν_1, ν_2, ν_3, K_a and K_c). However, these quantum numbers are not always known or, indeed, always valid [67].

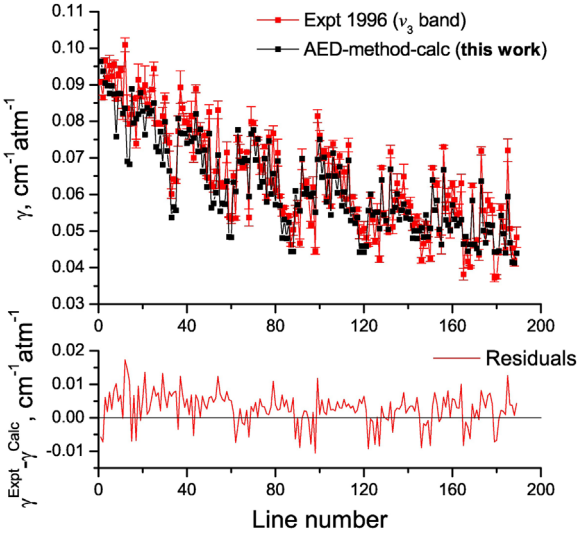

Fig. 2. Comparison of reconstructed $H_2{}^{16}O$-H_2 pressure dependent line widths with experimental values for the ν_3 band [34] at 296 K.

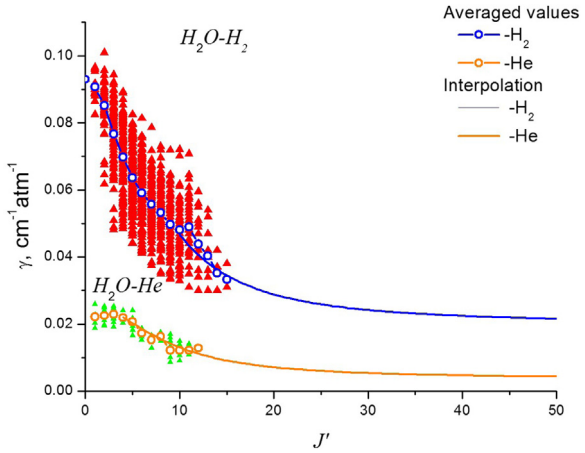

Fig. 3. Dependence of $H_2{}^{16}O$-H_2 and $H_2{}^{16}O$-He broadening coefficients on J' at 296 K.

For cases where only good quantum numbers (J and Γ_{tot}) are defined, the $J' - J''$ dependence technique can be applied. Available widths are compiled and averaged for each value of J' per branch (P, Q and R) and total symmetry (ortho/para). The resulting values are used to derive functions which describe the dependence of the averaged width on J' per branch and per symmetry (if there is appreciable difference for the latter two). This method applied to $H_2{}^{16}O$-H_2 and $H_2{}^{16}O$-He is illustrated in Fig. 3.

3.2. The $H_2{}^{16}O$-H_2 and $H_2{}^{16}O$-He line widths

Both approaches described in the previous section were used to obtain separate $H_2{}^{16}O$-H_2 and $H_2{}^{16}O$-He Lorentzian half-widths for BT2 lines in the range 500–10,000 cm^{-1} with an intensity that exceeds 1×10^{-30} cm/molecule in the temperature range 300–2000 K. Vibrational dependence is neglected as it is found to change the value of the half-widths by only a few percent. Dependence on K_c and total symmetry was found to be much smaller than dependence on K_a and $J' - J''$ respectively.

Our calculated values range between 0.0208 and 0.0927 cm^{-1} atm^{-1} for broadening by H_2 and 0.0043–0.0229 cm^{-1} atm^{-1} for broadening by He at 296 K. The average ratio between the H_2 to He pressure induced line widths is 4.2. Broadening of water by H_2 is much stronger than by He because the H_2 molecule has a quadrupole moment. The electrostatic potential is given by an expansion of the charge distribution in terms of the electric moments of the molecules. So, the main contribution into H_2O–H_2 broadening value is from the dipole-quadrupole interaction, besides this term there is also a quadrupole–quadrupole interaction contribution. Helium does not have any electric moments, so only the polarization potential (interactions between induced moments) gives the contribution, which is very much weaker.

Tables 1 and 2 present a summary of the comparison of our calculated values with available experimental and previous theoretical studies. The root mean square deviations (RMSD) between this work and other works is given as a percentage of the current values. For the $H_2{}^{16}O$-H_2 system the RMSD is within 20% or the uncertainty quoted in the given reference for all studies. It should be noted that for the comparison to Zeninari et al., the RMSD of 19.1 % is mainly down to the $6_{60} \leftarrow 6_{61}$ transition which is in fact an unresolved doublet [39]. The RMSD for the remaining five transitions is 8.4 %.

For the $H_2{}^{16}O$-He system the RMSD is within 26 % for all studies. Again for the comparison to Zeninari et al. , the RMSD of 15.0 % is mainly down to the $6_{60} \leftarrow 6_{61}$ transition. The RMSD for the

Table 1
Root mean square deviations (RMSD) of calculated values from available data on $H_2{}^{16}O$-H_2 broadening; γ is the half-width and n the temperature exponent. In many cases there are no experimental data available for comparison.

Reference	Number of transitions	RMSD γ (%)	RMSD n
Experiment			
Steyert et al. [35]	39	10.4	–
Brown and Plymate et al. [34]	630	7.4	–
Brown et al. [36]	4	8.8	–
Golubiatnikov [37]	1	13.9	–
Zeninari et al. [39]	6	19.1	–
Langlois et al. [41]	11	17	36.9 %
Dutta et al. [42]	2	7.3	–
Theory			
Gamache et al. [43]	386	6.2	
	32		4.9 %
Faure et al. [44]	228	24.1	18.2 %

Table 2
Root mean square deviations (RMSD) of calculated values from available data on $H_2{}^{16}O$-He broadening; γ is the half-width and n the temperature exponent.

Reference	Number of transitions	RMSD γ (%)	RMSD n
Experiment			
Petrova et al. [48]	103	17.1	–
Petrova et al. [47]	150	17.7	–
Petrova et al. [46]	105	15.5	–
Solodov and Starikov [49]	32	14.0	–
Solodov and Starikov [50]	53	13.9	–
Goyette and De Lucia [51]	1	1.7	42.2 %
Godon and Bauer [52]	2	10.3	13.6 %
Poddar et al. [54]	14	14.0	–
Claveau and Valentin [56]	10	25.7	–
Claveau et al. [55]	14	24.7	–
Steyert et al. [35]	39	23.3	–
Brown et al. [36]	4	11.1	–
Dutta et al. [42]	2	9.2	–
Zeninari et al. [39]	6	15.0	–
Golubiatnikov [37]	1	4.0	–
Lazarev et al. [53]	1	7.1	–
Theory			
Gamache et al. [43]	386	6.2	
	32		4.9 %

remaining five transitions is 8.6 %.

3.3. Temperature and pressure dependence of the $H_2{}^{16}O$-H_2/He line widths

In order to determine the temperature dependence, the half-width calculations were made at the following temperatures: T=300, 400, 500, 600, 700, 800, 900, 1000, 1200, 1400, 1600, 1800, 2000 K. The temperature dependence, represented by exponent n, was obtained by fitting to the standard relation:

$$\gamma(T) = \gamma_{\rm ref} \times \left(\frac{T_{\rm ref}}{T}\right)^n. \quad (2)$$

where $T_{\rm ref}$ = 296 K is the reference temperature, $\gamma_{\rm ref}$ is the Lorentzian half-width at reference temperature and n is the temperature exponent. The temperature exponents vary from 0.866 to 0.027 for broadening by H_2 and from 0.5 to 0.02 for broadening by He. Comparisons with experimentally derived and previously calculated values are summarised in Tables 1 and 2.

Recently Wilzewski et al. [68] commented that a single power law of the form Eq. (2) only works well within relatively narrow temperature intervals. However they also note that there is not enough experimental data to characterise an alternative model at present, and we find Eq. (2) reproduces our calculated values for the temperature range 300–2000 K to sufficient accuracy (within 3%). For high accuracy treatments other issues arise with use of the Voigt profile [69].

The pressure dependence of the Lorentzian half-widths in the range 0.001 - 10 bar is assumed to be linear:

$$\gamma(P) = \gamma_{\rm ref} \times \left(\frac{P}{P_{\rm ref}}\right). \quad (3)$$

where $P_{\rm ref}$=1 bar is the reference pressure. This is indicated by available pressure dependent experimental investigations up to around ambient pressure for broadening by H_2 [39], and up to around 3 atmospheres (≈ 3 bar) for broadening by He [47,48]. Although measurements at the high end of the pressure range (~10 bar) would be helpful to verify this; in particular high pressure leads to three-body effects which are implicitly neglected in our formulation.

3.4. The .broad files

In principle parameters were calculated for around 4 million BT2 lines with an intensity that exceeds 1×10^{-30} cm/molecule in the temperature range 300–2000 K. In practice, since vibrational dependence was neglected and dependence on total symmetry and rotational quantum number K_c was found to be comparatively small, the results comprise of around 23,000 widths that depend on J', J'', K_a' and K_a'', and 100 widths that depend on J' and J'' only. This can be represented in new ExoMol format [3] as two `.broad` files:

`1H2-16O__H2__NLAD.broad`, extract shown in Table 3.
`1H2-16O__He__NLAD.broad`, extract shown in Table 4.

These files and Eq. (4) below can be used to generate a pressure and temperature dependent Lorentzian half-width for any water vapour line, with at least $J' - J''$ quantum assignments, for a pure H_2, pure He or mixed H_2/He environment.

$$\gamma(T,P) = \left(\frac{T_{\rm ref}}{T}\right)^n \times \left(\frac{P}{P_{\rm ref}}\right) \times \sum_b \gamma_{{\rm ref},b} p_b. \quad (4)$$

where $\gamma_{{\rm ref},b}$ is the Lorentzian half-width due to a specific broadener

Table 3
`1H2-16O__H2__NLAD.broad`: Extract of $H_2{}^{16}O$-H_2 broad file: portion of the file (upper part); field specification (lower part).

a3	0.0690	0.502	5	4	1	3
a3	0.0580	0.424	6	6	3	3
a3	0.0754	0.541	3	3	0	1
…						
a1	0.0342	0.253	14	15		
a1	0.0328	0.241	15	16		
a1	0.0317	0.240	16	17		
…						

Field	Fortran format	C format	Description
Code	A2	% 2s	Code identifying quantum number set following J''*
$\gamma_{\rm ref}$	F6.4	%6.4f	Lorentzian half-width at reference temperature and pressure in cm^{-1}/bar
n	F5.3	%5.3f	Temperature exponent
J''	I7	% 7d	Lower J-quantum number
J'	I7	% 7d	Upper J-quantum number
K_a''	I2	% 2d	Lower rotational quantum number
K_a'	I2	% 2d	Upper rotational quantum number

* Code definitions: a3=parameters presented as a function of J'' (compulsory) and J', K_a'' and K_a'. a1=parameters presented as a function of J'' (compulsory) and J'.

Table 4
1H2-16O__He__NLAD.broad: extract of $H_2{}^{16}O$-He broad file: portion of the file (upper part); field specification (lower part).

a3	0.0213	0.269	5	4	1	3
a3	0.0183	0.241	6	6	3	3
a3	0.0226	0.320	3	3	0	1
…						
a1	0.0092	0.179	14	15		
a1	0.0086	0.145	15	16		
a1	0.0082	0.148	16	17		
…						

Field	Fortran format	C format	Description
Code	A2	% 2 s	Code identifying quantum number set following J''*
γ_{ref}	F6.4	%6.4f	Lorentzian half-width at reference temperature and pressure in cm^{-1}/bar
n	F5.3	%5.3f	Temperature exponent
J''	I7	% 7d	Lower J-quantum number
J'	I7	% 7d	Upper J-quantum number
K_a''	I2	% 2d	Lower rotational quantum number
K_a'	I2	% 2d	Upper rotational quantum number

* Code definitions: a3 = parameters presented as a function of J'' (compulsory) and J', K_a'' and K_a'. a1 = parameters presented as a function of J'' (compulsory) and J'.

in units cm^{-1}/bar (ExoMol convention) and p_b is the partial pressure of the broadener. Note that to convert from cm^{-1}/bar used by ExoMol to cm^{-1}/atm used by Hitran requires γ to be multiplied by 1.01325.

The .broad files presented as part of this work differ slightly from those included in the ExoMol database. The .broad files provided with the ExoMol line lists, described in [3], contain data from multiple sources while the .broad files available as supplementary data to this work contain data from only one source, the current work. Hence, the file names are appended with a dataset name NLAD. We recommend the use of the full .broad file presented on the ExoMol website as this includes both line-by-line parameters where available, which are essential for detailed and high resolution studies, while the current model which allows a width to be generated for every molecular line.

4. Computation of $H_2{}^{16}O$ absorption cross-sections

4.1. Method

The high resolution cross section is calculated on an evenly spaced wavenumber grid, $\tilde{\nu}_i$, defining bins of width $\Delta\tilde{\nu}$. A Voigt profile is used to model the joint contributions from thermal and collision induced broadening:

$$f_V(\tilde{\nu}, \tilde{\nu}_{0;j}, \alpha_j, \gamma_j) = \frac{1}{\sqrt{\pi}} \frac{\sqrt{\ln 2}}{\alpha_j} \mathrm{wofz}\left(\frac{\tilde{\nu} - \tilde{\nu}_{0;j}}{\alpha_j} \sqrt{\ln 2} + i \frac{\gamma_j}{\alpha_j} \sqrt{\ln 2} \right) \quad (5)$$

where wofz is the scaled complex complementary error function, also known as the Faddeeva function. This is calculated using the Faddeeva package [70]. $\tilde{\nu}_{0;j}$ is the line centre, γ_j is the Lorentzian half-width at half-maximum and α_j is the Doppler half-width at half-maximum given by:

$$\alpha = \sqrt{\frac{2kT \ln 2}{m}} \frac{\tilde{\nu}_{0;j}}{c} \quad (6)$$

at temperature T in K for a molecule of mass m in kg. Note that in the limit $\alpha \gg \gamma$, the profile reduces to a Gaussian:

$$f_G(\tilde{\nu}, \tilde{\nu}_{0;j}, \alpha_j) = \sqrt{\frac{\ln 2}{\pi}} \frac{1}{\alpha_j} \exp\left(-\frac{(\tilde{\nu} - \tilde{\nu}_{0;j})^2 \ln 2}{\alpha_j^2} \right) \quad (7)$$

whereas for $\alpha \ll \gamma$ the profile reduces to a Lorentzian:

$$f_L(\tilde{\nu}, \tilde{\nu}_{0;j}, \gamma_j) = \frac{\gamma_j}{\pi} \frac{1}{(\tilde{\nu} - \tilde{\nu}_{0;j})^2 + \gamma_j^2} \quad (8)$$

However a Voigt profile is evaluated for every absorption line in all calculations of cross sections presented in this work. The cross section for each bin is the sum of the contributions from individual lines:

$$\sigma_i = \sum_j \sigma_{ij} \quad (9)$$

where:

$$\sigma_{ij} = S_j f_V(\tilde{\nu}, \tilde{\nu}_{0;j}, \alpha_j, \gamma_j). \quad (10)$$

S_j is the line intensity in units of cm per molecule given by:

$$S_j = \frac{A_j}{8\pi c} \frac{g_j' \exp\left(-c_2 E_j''/T\right)}{\tilde{\nu}_{0;j}^2 Q(T)} \left(1 - \exp\left(-\frac{c_2 \tilde{\nu}_{0;j}}{T}\right)\right) \quad (11)$$

Here, g_j' and E_j'' are the total upper-state degeneracy and lower-state energy respectively, A_j is the Einstein A coefficient for the transition and $c_2 = hc/k_B$ is the second radiation constant. $\tilde{\nu}_{0;j}$ and A_j were taken from the BT2 line list while the molecular partition function, $Q(T)$, was obtained from the tabulated values of Vidler and Tennyson [71].

When evaluating a Voigt profile it is necessary to select an appropriate profile grid resolution and evaluation width in order to adequately sample the contribution from the profile whilst considering the computational cost. For the profile grid resolution we adopted the staggered wavenumber grid spacings of [33] (see Table 5). These spacings are well below the Voigt width for the pressure and temperature range considered, which is essential for Eq. (10) to be valid.

For the profile evaluation width we adopted a cut-off of $200 \times (\alpha_j + \gamma_j)$ either side of the centroid. We find that this is sufficient to capture the contributions from the wings in a manner that adapts with both pressure and temperature.

We note Hedges and Madhusudhan [72] recently investigated the effect of various factors, including the profile grid resolution and evaluation width, on pressure dependent absorption cross sections for application to exoplanet atmospheres. Hedges and Madhusudhan proposed a more computationally-efficient grid resolution, a pressure adaptive grid, than the staggered grid employed by this work. However, they comment that the pressure adaptive grid resulted in a small loss of opacity (~2%) compared to the staggered grid at the high end of the pressure range (P ~10 bar). Hence we opted for the staggered grid. For the profile evaluation width Hedges and Madhusudhan compared two methods, a pressure adaptive fixed cut-off and a cut-off evaluated per line as a multiple of Lorentzian half-widths, to their approach, a cut-off evaluated per line as a multiple of effective Voigt

Table 5
Summary of the grid spacings for the cross sections calculated in difference wavenumber regions.

Wavenumber range cm^{-1}	Grid spacing cm^{-1}
10–100	10^{-5}
100–1000	10^{-4}
1000–10,000	10^{-3}
10,000–30,000	10^{-2}

Table 6
Temperatures and pressures at which $H_2{}^{16}O$ cross sections are calculated.

Temperature (K)			
300	400	500	600
700	800	900	1000
1200	1400	1600	1800
2000			
Pressure (bar)			
0.001	0.003	0.005	0.01
0.02	0.04	0.08	0.1
0.3	0.6	0.9	1.0
1.2	1.5	2.0	2.5
3.0	4.0	5.0	6.0
8.0	10.0		

half-widths. Their effective Voigt half-width was defined as [72]:

$$\gamma_V \approx 0.5346\gamma_L + \sqrt{0.2166\gamma_L^2 + \gamma_G^2} \tag{12}$$

where $\gamma_G = \alpha_j$, $\gamma_L = \gamma_j$ and $\gamma_V < (\alpha_j + \gamma_j)$ for comparison to this work. Hedges & Madhusudhan found that both the fixed cut-off method and Lorentzian half-width analysis resulted in significant (>40%) opacity loss at the low end of the pressure range (P <0.01 bar) compared to the Voigt half-width analysis. As our approach is very similar to Hedges & Madhusudhan we should also avoid this loss of opacity.

4.2. Results

Pressure dependent absorption cross sections for $H_2{}^{16}O$ in a mixed H_2/He environment (85/15% by number) are calculated on a fixed temperature and pressure grid (see Table 6) using the BT2 line list, pressure broadening parameters determined as part of this work (Section 1) and the method described above. However, no attempt is made include contributions to the opacity from the water vapour continuum or water dimer absorption.

The cross sections were calculated between 10 and 30,000 cm^{-1} using the staggered wavenumber grid given in Table 5 and then binned to a common grid spacing of 0.01 cm^{-1}. Each region was calculated to overlap with its neighbours by at least 1 cm^{-1}, which we find to be sufficient to avoid discontinuities when they are binned to a common grid spacing.

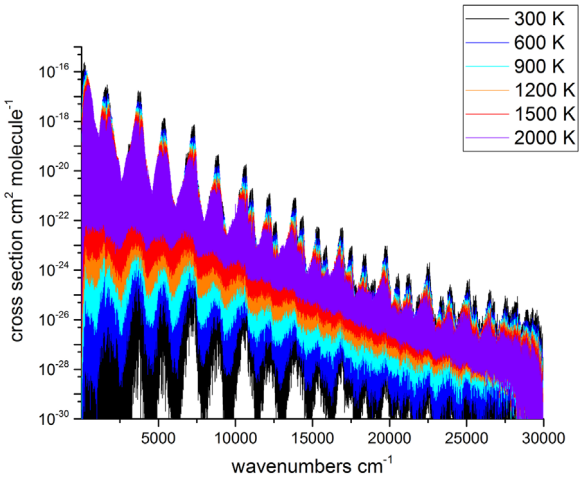

Fig. 4. $H_2{}^{16}O$ cross sections in a mixed H_2–He (85/15%) environment calculated at 0.01 bar and temperatures in the range 300–2000 K. A cut-off of 200 × $(\alpha_j + \gamma_j)$ was used (see text).

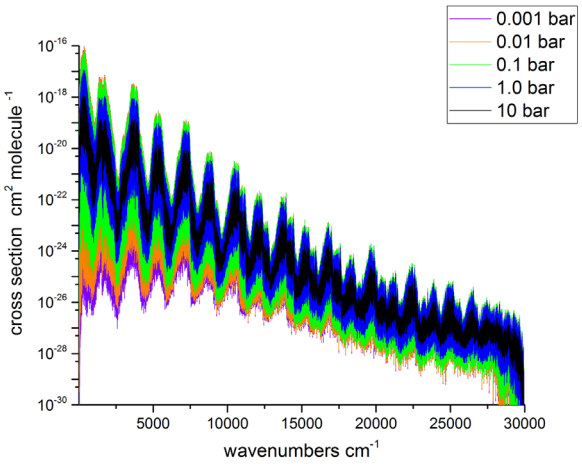

Fig. 5. $H_2{}^{16}O$ cross sections in a mixed H_2–He (85/15%) environment calculated at 1000 K and pressures in the range 0.001–10 bar. A cut-off of 200 ×$(\alpha_j + \gamma_j)$ was used (see text).

Calculated cross sections for a range of temperatures at a single pressure and a range of pressures at a single temperature are shown in Figs. 4 and 5. A change in temperature predominately influences the shape of the cross section (Fig. 4) while a change in pressure results in a redistribution of opacity (Fig. 5).

4.3. Interpolation of cross-sections between temperatures and pressures

Cross sections are provided for 12 temperatures and 22 pressures between 300 and 2000 K and 0.001 and 10 bar respectively (see Table 6). A cross section at intermediate conditions may be obtained by first interpolating on the temperature grid using either Eqs. (14) or (16) below [33], then interpolating on the pressure grid using Eq. (19) below. The interpolation residual is expressed as a percentage of the corresponding absorption cross-section:

$$\delta\sigma_{\max}^{\%} = \max\left(\frac{|\sigma_{i,calc} - \sigma_{i,interp}|}{\sigma_{i,calc}}\right) \times 100 \tag{13}$$

To obtain cross sections at an intermediate temperature T, interpolation between cross sections computed for a higher temperature T_2 and a lower temperature T_1 may be performed linearly [33]:

$$\sigma_i = \sigma_i(T_1) + m(T - T_1) \tag{14}$$

where:

$$m = \frac{\sigma_i(T_2) - \sigma_i(T_1)}{T_2 - T_1} \tag{15}$$

Or using a more accurate exponential model [33]:

$$\sigma_i = a_i e^{\frac{b_i}{T}}, \tag{16}$$

where:

$$b_i = \left(\frac{1}{T_2} - \frac{1}{T_1}\right)^{-1} \ln\frac{\sigma_i(T_1)}{\sigma_i(T_2)}, \tag{17}$$

and:

$$a_i = \sigma_i(T_1) e^{\frac{b_i}{T}} \tag{18}$$

The error in the cross sections introduced by the more accurate interpolation scheme does not exceed 1.64% which is less than the estimated uncertainty in the *ab initio* line lists.

To obtain cross sections at an intermediate pressure P, interpolation between cross sections computed for a higher pressure P_2 and a lower pressure P_1 may be performed linearly:

$$\sigma_i = \sigma_i(P_1) + m(P - P_1) \quad (19)$$

where:

$$m = \frac{\sigma_i(P_2) - \sigma_i(P_1)}{P_2 - P_1} \quad (20)$$

This results in interpolation residuals below 2.6% for the region 6000–30,000 cm^{-1} for all pressures. However, below 6000 cm^{-1} for low pressures and below 1000 cm^{-1} for high pressures, there are spikes in interpolation residual (>10%) for individual wavenumber bins, notably in the wings of strong features. The wings of strong lines add appreciable amounts of opacity to wavenumber bins where there previously was negligible opacity in an non-linear fashion. In reality this effects only a small fraction of the bins (~0.7%) and changes the total cross section in the region 10–6000 cm^{-1} by less than 0.002 % at worst, hence this should have negligible effect on practical applications.

5. Conclusion

$H_2{}^{16}O$ line widths pressure-broadened by hydrogen and helium were calculated using the averaged energy difference method and J' J''-dependence technique. Rotational quantum numbers J up to 50 were considered. The temperature dependence of the widths was derived from calculations made at temperatures in the range 300–2000 K. The calculated data are in reasonable agreement with available experiment.

The widths and temperature exponents are presented in the new ExoMol format as dataset exclusive `.broad` files and can be used to generate a temperature and pressure dependent Lorentzian-half width for every line of the BT2 line list, or any line list with at least $J' - J''$ assignments.

High resolution pressure dependent absorption cross sections for $H_2{}^{16}O$ have been calculated for a mixed H_2/He (85/15% by number) environment and a range of temperatures (T=300–2000 K) and pressures (P=0.001–10 bar) relevant to exoplanet and cool star atmospheres. The static cross sections are available from the ExoMol website (www.exomol.com/data/molecules/H2O/1H2-16O/BT2/).

It is our intention to make the cross sections available through the ExoMol cross section service, a web-based interface (www.exomol.com/data/data-types/xsec/) which currently allows astronomers to download zero pressure cross sections for available molecules at user defined temperatures and spectral resolution.

The form chosen for representing the pressure-broadening parameters is based on the quantum numbers of the upper and lower levels. This means that the parameters are transferable to other extensive water line lists such as new, complete and more accurate POKAZATEL line list [73] which will be released soon. Furthermore, the differences in pressure effects between $H_2{}^{16}O$, and $H_2{}^{17}O$ and $H_2{}^{18}O$ should be very small. This means that the broadening files presented here should also be appropriated for the newly computed $H_2{}^{17}O$ and $H_2{}^{18}O$ hot line lists [74].

Pressure dependent absorption cross sections for other key species in the atmospheres of exoplanets and cool stars (for example NH_3, CO, CO_2 and CH_4) will also be included here in due course [75].

Acknowledgements

This work was supported by a grant from Energinet.dk project N. 2013-1-1027, by UCL through the Impact Studentship Program and the European Research Council under Advanced Investigator Project 267219 and partly supported by CNRS in the frame of the International Associated Laboratory SAMIA and RFBR No. 16-32-00244.

References

[1] Tennyson J, Yurchenko SN. ExoMol: molecular line lists for exoplanet and other atmospheres. Mon Not R Astron Soc 2012;425:21–33.
[2] Tinetti G, Tennyson J, Griffiths CA, Waldmann I. Water in exoplanets. Philos Trans R Soc Lond A 2012;370:2749–2764.
[3] Tennyson J, Yurchenko SN, Al-Refaie AF, Barton EJ, Chubb KL, Coles PA, et al. The ExoMol database: molecular line lists for exoplanet and other hot atmospheres. J Mol Spectrosc 2016;327:73–94. http://dx.doi.org/10.1016/j.jms.2016.05.002.
[4] Tinetti G, Encrenaz T, Coustenis A. Spectroscopy of planetary atmospheres in our galaxy. Astron Astrophys Rev 2013;21:1–65. http://dx.doi.org/10.1007/s00159-013-0063-6.
[5] Crossfield IJM. Observations of exoplanet atmospheres. Publ Astron Soc Pac 2015;127:956.
[6] Tinetti G, Vidal-Madjar A, Liang M-C, Beaulieu J-P, Yung Y, Carey S, et al. Water vapour in the atmosphere of a transiting extrasolar planet. Nature 2007;448:169–171.
[7] Swain MR, Deroo P, Griffith CA, Tinetti G, Thatte A, Vasisht G, et al. A ground-based near-infrared emission spectrum of the exoplanet HD 189733b. Nature 2010;463:637–639.
[8] Swain MR, Vasisht G, Tinetti G, Bouwman J, Chen P, Yung Y, et al. Molecular signatures in the near-infrared dayside spectrum of HD 189733b. Astrophys J 2009;690:L114–L117. http://dx.doi.org/10.1088/0004-637X/690/2/L114.
[9] Birkby JL, de Kok RJ, Brogi M, de Mooij EJW, Schwarz H, Albrecht S, et al. Detection of water absorption in the day side atmosphere of HD 189733 b using ground-based high-resolution spectroscopy at 3.2 mu m. Mon Not R Astron Soc 2013;436:L35–L39. http://dx.doi.org/10.1093/mnrasl/slt107.
[10] McCullough PR, Crouzet N, Deming D, Madhusudhan N. Water vapor in the spectrum of the extrasolar planet HD 189733b. I. The transit. Astrophys J 2014;791:55. http://dx.doi.org/10.1088/0004-637X/791/1/55.
[11] Todorov KO, Deming D, Burrows A, Grillmair CJ. Updated spitzer emission spectroscopy of bright transiting hot jupiter HD 189733b. Astrophys J 2014;796:100. http://dx.doi.org/10.1088/0004-637X/796/2/100.
[12] Stevenson KB, Harrington J, Nymeyer S, Madhusudhan N, Seager S, Bowman WC, et al. Possible thermochemical disequilibrium in the atmosphere of the exoplanet GJ 436b. Nature 2010;464:1161–1164.
[13] Knutson HA, Madhusudhan N, Cowan NB, Christiansen JL, Agol E, Deming D, et al. A Spitzer transmission spectrum for the exoplanet GJ 436b, evidence for stellar variability, and constraints on dayside flux variations. Astrophys J 2011;735:27. http://dx.doi.org/10.1088/0004-637X/735/1/27.
[14] Beaulieu JP, Kipping DM, Batista V, Tinetti G, Ribas I, Noriega-Crespo SCJA, et al. Water in HD 209458b's atmosphere from 3.6 to 8 μ m IRAC photometric observations in primary transit. Mon Not R Astron Soc 2010;409:963–974.
[15] Deming D, Wilkins A, McCullough P, Burrows A, Fortney JJ, Agol E, et al. Infrared transmission spectroscopy of the exoplanets HD 209458b and XO-1b using the wide field camera-3 on the hubble space telescope. Astrophys J 2013;774:95. http://dx.doi.org/10.1088/0004-637X/774/2/95.
[16] Tinetti G, Deroo P, Swain MR, Griffith CA, Vasisht G, Brown LR, et al. Probing the terminator region atmosphere of the hot-jupiter XO-1b with transmission spectroscopy. Astrophys J Lett 2010;712:L139–L142. http://dx.doi.org/10.1088/2041-8205/712/2/L139.
[17] Wakeford HR, Sing DK, Deming D, Gibson NP, Fortney JJ, Burrows AS, et al. HST hot Jupiter transmission spectral survey: detection of water in HAT-P-1b from WFC3 near-IR spatial scan observations. Mon Not R Astron Soc 2013;435:3481–3493. http://dx.doi.org/10.1093/mnras/stt1536.
[18] Brogi M, de Kok RJ, Birkby JL, Schwarz H, Snellen IAG. Carbon monoxide and water vapor in the atmosphere of the non-transiting exoplanet HD 179949 b. Astron Astrophys 2014;565:A124. http://dx.doi.org/10.1051/0004-6361/201423537.
[19] Huitson CM, Sing DK, Pont F, Fortney JJ, Burrows AS, Wilson PA, et al. An HST optical-to-near-IR transmission spectrum of the hot Jupiter WASP-19b: detection of atmospheric water and likely absence of TiO. Mon Not R Astron Soc 2013;434:3252–3274. http://dx.doi.org/10.1093/mnras/stt1243.
[20] Kreidberg L, Line MR, Bean JL, Stevenson KB, Desert J-M, Madhusudhan N, et al. A detection of water in the transmission spectrum of the hot Jupiter WASP-12b and implications for its atmospheric composition. Astrophys J 2015;814:66. http://dx.doi.org/10.1088/0004-637X/814/1/66.
[21] Konopacky QM, Barman TS, Macintosh BA, Marois C. Detection of carbon monoxide and water absorption lines in an exoplanet atmosphere. Science 2013;339:1398–1401. http://dx.doi.org/10.1126/science.1232003.
[22] Barman TS, Konopacky QM, Macintosh B, Marois C. Simultaneous detection of

water, methane, and carbon monoxide in the atmosphere of exoplanet HR8799 b. Astrophys J 2015;804:61. http://dx.doi.org/10.1088/0004-637X/804/1/61.
[23] Sharp CM, Burrows A. Atomic and molecular opacities for brown dwarf and giant planet atmospheres. Astrophys J Suppl 2007;168:140.
[24] Bernath PF. Molecular astronomy of cool stars and sub-stellar objects. Int Rev Phys Chem 2009;28:681–709. http://dx.doi.org/10.1080/01442350903292442.
[25] Allard F, Homeier D, Freytag B. Models of very-low-mass stars, brown dwarfs and exoplanets. Philos Trans R Soc Lond A 2012;370:2765–2777. http://dx.doi.org/10.1098/rsta.2011.0269.
[26] Morley CV, Marley MS, Fortney JJ, Lupu R, Saumon D, Greene T, et al. Water clouds in y dwarfs and exoplanets. Astrophys J 2014;787:78. http://dx.doi.org/10.1088/0004-637X/787/1/78.
[27] Allard F, Hauschildt PH, Miller S, Tennyson J. The influence of H_2O line blanketing on the spectra of cool dwarf stars. Astrophys J 1994;426:L39–L41.
[28] Faherty JK, Tinney CG, Skemer A, Monson AJ. Indications of water clouds in the coldest known brown dwarf. Astrophys J 2014;793:L16.
[29] Skemer AJ, Morley CV, Allers KN, Geballe TR, Marley MS, Fortney JJ, et al. The first spectrum of the coldest brown dwarf. Astrophys J Lett 2016;826:L17. http://dx.doi.org/10.3847/2041-8205/826/2/L17.
[30] Rothman LS, Gordon IE, Barber RJ, Dothe H, Gamache RR, Goldman A, et al. HITEMP, the high-temperature molecular spectroscopic database. J Quant Spectrosc Radiat Transf 2010;111:2139–2150.
[31] Gordon IE, Rothman LS, Gamache RR, Jacquemart D, Boone C, Bernath PF, et al. Current updates of the water-vapor line list in HITRAN: a new diet for air-broadened half-widths. J Quant Spectrosc Radiat Transf 2007;108:389–402. http://dx.doi.org/10.1016/j.jqsrt.2007.06.009.
[32] Barber RJ, Tennyson J, Harris GJ, Tolchenov RN. A high accuracy computed water line list. Mon Not R Astron Soc 2006;368:1087–1094.
[33] Hill C, Yurchenko SN, Tennyson J. Temperature-dependent molecular absorption cross sections for exoplanets and other atmospheres. Icarus 2013;226:1673–1677.
[34] Brown LR, Plymate C. H_2-broadened $H^{216}O$ in four infrared bands between 55 and 4045 cm^{-1}. J Quant Spectrosc Radiat Transf 1996;56:263–282. http://dx.doi.org/10.1016/0022-4073(95)00191-3.
[35] Steyert DW, Wang W, Sirota J, Donahue NM, Reuter DC. Hydrogen and helium pressure broadening of water transitions in the 380–600 cm^{-1} region. J Quant Spectrosc Radiat Transf 2004;83:183–191. http://dx.doi.org/10.1016/S0022-4073(02)00300-X.
[36] Brown LR, Benner DC, Devi VM, Smith MAH, Toth RA. Line mixing in self- and foreign-broadened water vapor at 6 microns. J Mol Struct 2005;742:111–122.
[37] Golubiatnikov YG. Shifting and broadening parameters of the water vapor 183-GHz line (3_{13}-2_{20}) by H_2O, O_2, N_2, CO_2, H_2, He, Ne, Ar, and Kr at room temperature. J Mol Spectrosc 2005;230:196–198.
[38] Lucchesinia A, Gozzini S, Gabbanini C. Water vapor overtones pressure line broadening and shifting measurements. Eur Phys J D 2000;8:223–226.
[39] Zeninari V, Parvitte B, Courtois D, Lavrentieva NN, Ponomarev YN, Durry G. Pressure broadening and shift coefficients of H_2O due to perturbation by N_2, O_2, H_2 and He in the 1.39 micron region: experiment and calculations. Mol Phys 2004;102:1697–1706.
[40] Dick MJ, Drouin BJ, Pearson JC. A collisional cooling investigation of the pressure broadening of the 1_{10}-1_{01} transition of water from 17 to 200 K. J Quant Spectrosc Radiat Transf 2009;110:619–627. http://dx.doi.org/10.1016/j.jqsrt.2008.11.012.
[41] Langlois S, Birbeck TP, Hanson RK. Temperature-dependent collision-broadening parameters of h_2o lines in the 1.4 μm region using diode laser absorption spectroscopy. J Mol Spectrosc 1994;167:272–281. http://dx.doi.org/10.1006/jmsp.1994.1234.
[42] Dutta JM, Jones CR, Goyette TM, Lucia FC. The hydrogen and helium pressure broadening at planetary temperatures of the 183 and 380 GHz transitions of water vapor. Icarus 1993;102:232–239.
[43] Gamache RR, Lynch R, Brown LR. Theoretical calculations of pressure broadening coefficients for H_2O perturbed by hydrogen or helium gas. J Quant Spectrosc Radiat Transf 1996;56:471–487. http://dx.doi.org/10.1016/0022-4073(96)00098-2.
[44] Faure A, Wiesenfeld L, Tennyson J, Drouin BJ. Pressure broadening of water and carbon monoxide transitions by molecular hydrogen at high temperatures. J Quant Spectrosc Radiat Transf 2013;116:79–86.
[45] Drouin B, Wiesenfeld L. Low-temperature water hydrogen-molecule collisions probed by pressure broadening and line shift. Phys Rev A 2012;86:022705.
[46] Petrova TM, Solodov AM, Solodov AA, Starikov VI. Measurements and calculations of He-broadening and -shifting parameters of the transitions of the $\nu_1+\nu_2+\nu_3$ bands. Mol Phys 2012;110:1493–1503.
[47] Petrova TM, Solodov AM, Solodov AA, Starikov VI. Vibrational dependence of an intermolecular potential for H_2O-He system. J Quant Spectrosc Radiat Transf 2013;129:241–253.
[48] Petrova TM, Solodov AM, Solodov AA, Starikov VI. Broadening parameters of the H_2O-He collisional system for astrophysical applications. J Mol Spectrosc 2016;321:50–58.
[49] Solodov AM, Starikov VI. Broadening and shift lines of the $\nu_2+\nu_3$ band of water vapour induced by helium pressure. Opt Spectrosc 2008;105:14–20.
[50] Solodov AM, Starikov VI. Helium-induced half widths and line shifts of water vapour transitions of the $\nu_1+\nu_2$ and $\nu_2+\nu_3$ bands. Mol Phys 2009;104:43–51.
[51] Goyette TM, Lucia FCD. The pressure broadening of the 3_{13}-2_{20} transition of water between 80 and 600 K. J Mol Spectrosc 1990;143:346–358.
[52] Godon M, Bauer A. Helium-broadened widths of the 183 and 380 GHz lines of water vapour. Chem Phys Lett 1988;147:189–191.
[53] Lazarev VV, Ponomarev YN, Sumpf B, Fleischmann O, Waschull J, Kronfeldt H, et al. Noble gas pressure-induced broadening and shift of H_2O and SO_2 absorption lines. J Mol Spectrosc 1995;173:177–193.
[54] Poddar P, Mitra S, Hossain MM, Biswas D, Ghosh PN, Ray B. Diode laser spectroscopy of He, N_2 and air broadened water vapour transitions belonging to the $2\nu_1+\nu_2+\nu_3$ overtone band. Mol Phys 2010;108:1957–1964.
[55] Claveau C, Henry A, Hurtmans D, Valentin A. Narrowing and broadening parameters of H_2O lines perturbed by He, Ne, Ar, Kr and nitrogen in the spectral range 1850–2140 cm^{-1}. J Quant Spectrosc Radiat Transf 2001;68:273–298.
[56] Claveau C, Valentin A. Narrowing and broadening parameters of H_2O lines perturbed by Helium, argon and xenon in the 1170–1440 cm^{-1} spectral range. Mol Phys 2009;107:1417–1422.
[57] Dicke RH. The effect of collisions upon the doppler width of spectral lines. Phys Rev 1953;86:472–473.
[58] Wittke JP, Dicke RH. Redetermination of the hyperfine splitting in the ground state of atomic hydrogen. Phys Rev 1956;103:620–631.
[59] Lavrentieva NN, Dudaryonok AS, Ma Q. Line broadening estimate from averaged energy differences of coupled states. Proc SPIE 92920M 2014:1–9.
[60] Voronin BA, Lavrentieva NN, Mishina TP, Chesnokova TY, Barber MJ, Tennyson J. Estimate of the $J'J''$ dependence of water vapour line broadening parameters. J Quant Spectrosc Radiat Transf 2010;111:2308–2314.
[61] Ma Q, Tipping RH, Boulet C. Modification of the Robert-Bonamy formalism in calculating Lorentzian half-widths and shifts. J Quant Spectrosc Radiat Transf 2007;103:588–596.
[62] Anthony BK, Gamache PR, Szembek CD, Niles DN, Gamache RR. Modified complex Robert-Bonamy formalism calculations for strong to weak interacting systems. Mol Phys 2006;104:1–9.
[63] Lynch R, Gamache RR, Neshyba SP. N_2 and O_2 induced half-widths and line shifts of water vapour lines in the (301) - (000) and (221) - (000). J Quant Spectrosc Radiat Transf 1998;59:595.
[64] Gamache RR, Lynch R, Neshyba SP. New developments in the theory of pressure-broadening and presure-shifting of spectral lines of H_2O: the complex robert-bonamy formalism. J Quant Spectrosc Radiat Transf 1998;59:319.
[65] Lynch R. Half-widths and line shifts of water vapour perturbed by both nirtogen and oxygen., [Ph.D. thesis]. Physics Department, University of Massachusetts Lowell; 1995.
[66] Hodges JT, Lisak D, Lavrentieva N, Bykov A, Sinitsa L, Tennyson J, et al. Comparison between theoretical calculations and high-resolution measurements of pressure-broadening for water vapor spectra near 935 nm. J Mol Spectrosc 2008;249:86–94.
[67] Child MS, Weston T, Tennyson J. Quantum monodromy in the spectrum of H_2O and other systems: new insight into the level structures of quasi-linear molecules. Mol Phys 1999;96:371–379.
[68] Wilzewski JS, Gordon IE, Kochanov RV, Hill C, Rothman LS. H_2, He, and CO_2 line-broadening coefficients, pressure shifts and temperature-dependence exponents for the HITRAN database Part 1: SO_2, NH_3, HF, HCl, OCS and C_2H_2. J Quant Spectrosc Radiat Transf 2016;168:193–206. http://dx.doi.org/10.1016/j.jqsrt.2015.09.003.
[69] Tennyson J, Bernath PF, Campargue A, Császár AG, Daumont L, Gamache RR, et al., Recommended isolated-line profile for representing high-resolution spectroscopic transitions (IUPAC Technical Report). Pure Appl Chem. Vol. 86; 2014. p. 1931–43.
[70] Johnson SG., The Faddeeva package. ⟨http://ab-initio.mit.edu/wiki/index.php/Faddeeva_Package⟩; 2012.
[71] Vidler M, Tennyson J. Accurate partition function and thermodynamic data for water. J Chem Phys 2000;113:9766–9771.
[72] Hedges C, Madhusudhan N. Effect of pressure broadening on molecular absorption cross sections in exoplanetary atmospheres. Mon Not R Astron Soc 2016;458(2):1427–1449. http://dx.doi.org/10.1093/mnras/stw278.
[73] Polyansky OL, Kyuberis AA, Lodi L, Tennyson J, Ovsyannikov RI, Zobov N, Yurchenko SN. ExoMol molecular line lists XXII: high accuracy computed line list for hot $H_2{}^{16}O$. Mon Not R Astron Soc. (to be submitted, 2017).
[74] Polyansky OL, Kyuberis AA, Lodi L, Tennyson J, Ovsyannikov RI, Zobov N. ExoMol molecular line lists XIX: high accuracy computed line lists for $H_2{}^{17}O$ and $H_2{}^{18}O$. Mon Not R Astron Soc. (in press, 2017).
[75] Barton EJ, Hill C, Czurylo M, Li H-Y, Hyslop A, Yurchenko SN, Tennyson J. The ExoMol diet of line-by-line pressure-broadening parameters. J Quant Spectrosc Radiat Transf.(to be submitted, 2017).